Retrieval of the Characteristic Size of Raindrops for Wind Sensing Based on Dual-Polarization Radar

Yunli Peng, Jianbing Li, *Senior Member, IEEE,* Jiapeng Yin, Pak Wai Chan, Wai Kong, and Xuesong Wang

***Abstract*—Wind velocity is of great importance for weather monitoring, aviation hazard alerting, wind energy exploring, and etc. Doppler radar is widely used to measure wind under rainy condition by sensing the raindrops entrained by the background wind. However, the Doppler velocity, which is a reflection of the raindrops' velocity in radial direction, is not coincident with the background wind because of the strong inertia of raindrops. Efforts should be made to distinguish the difference between the raindrops' velocity and the background wind velocity. In this paper, we try to establish a relationship between the background wind velocity and the raindrops' velocity by introducing a definition of the raindrops' characteristic size, which is related to the velocity characterized by the strongest Doppler spectral component. It is found that the fusion of differential reflectivity and the depolarization ratio can serve as a good proxy for the estimation of the characteristic size. Simulation results for S/C/X band radars and radar measurements verify the good performance of the proposed retrieval model for the characteristic size, which lays a solid foundation for the retrieval of the background wind velocity.**

***Index Terms*—Drop size distribution, equivalent RCS, characteristic size of raindrops, differential reflectivity, depolarization ratio, support vector regression.**

I. Introduction

THE information of wind is an important factor for weather monitoring, aviation hazard alerting, wind energy exploring, climate studies and etc., and the wind measurement technology has attracted much attention in the past decades. The instruments for wind detection over large spatial and temporal scales mainly include lidar and radar. Lidar is generally a good option for wind detection in dry air [1]–[3], but its application in wet weather condition is greatly limited due to the heavy propagation attenuation of laser in precipitations. Comparatively, radar performs well in wet weather condition because microwave radiation can propagate through the precipitation with much less attenuation. For ocean surface wind, remote sensing techniques were well investigated [4]–[9], where the main detection mechanism is to retrieve wind information based on the sensitivity of the ocean surface's scattering cross section to the changes of wind velocity. However, for inland wind sensing under rainy condition, the main mechanism is to retrieve the background wind velocity from the Doppler velocity of raindrops entrained by the wind [10]–[12]. However, the Doppler velocity, which is a reflection of the raindrops' velocity, is not coincident with the background wind velocity because of the strong inertia of raindrops [13]. This results in a gap between the background wind velocity and the raindrop's Doppler velocity, and efforts should be made to fix this gap.

It is known that for a certain radar range bin, the Doppler spectrum, which is composed of a lot of spectral components, reveals the ensembling effect of the dynamics of all the raindrops in this range bin. And the most typical method to obtain the Doppler velocity is to extract the velocity at the spectral component with the highest spectral energy. In this manner, if the size of the raindrops corresponding to the strongest Doppler spectral component can be determined, the motion equation of this group of raindrops can be established. This equation presents the relationship between the raindrops' velocity (reflected by the Doppler velocity) and the background wind velocity, making it possible to retrieve the background wind velocity with mathematical techniques. Therefore, a key issue for the above process is to get the raindrop's size for the strongest Doppler spectral component, which is also the main content of this paper.

In fact, raindrop size distribution (DSD) and its retrieval technology have been studied in meteorology community for a long time. Since Seliga and Bringi [14] indicated that the polarimetric variables can be used to retrieve the parameters of an exponential raindrop size distribution model in 1976, plenty of studies have been conducted to explore the relationship between polarimetric variables and raindrop's size. Among them, the Gamma distribution [15] and Normalized Gamma distribution [16] were widely used due to their good adaptability to different rain cases, such as the Constrained Gamma method [17] and the Beta method [18], [19]. And those methods have also been applied to data of different radar bands with the development of dual-polarization radar and the correction technology of attenuation effect.

Even though there have been a lot of efforts to get the DSD of raindrops, the retrieval of a special size that corresponding to the strongest Doppler spectral component has been rarely studied. This size can serve as a bridge to connect the raindrops' velocity (reflected by the Doppler velocity) and background wind velocity, so it is called the characteristic size in the present study. The main objectives of this study are:

1) to propose a new approach to retrieve the characteristic size directly;

2) to test the performance of retrieval models of the characteristic size with field observation data;

This work was supported by the National Natural Science Foundation of China under Grant 61771479. (Corresponding author: Jianbing Li.)

Yunli Peng, Jianbing Li, Jiapeng Yin and Xuesong Wang are with the State Key Laboratory of Complex Electromagnetic Environment Effects on Electronics and Information System, College of Electronic Science and Engineering, National University of Defense Technology, Changsha, Hunan, 410073, China(email:jianbingli@nudt.edu.cn).

Pak Wai Chan and Wai Kong are with the Hong Kong Observatory, 134A Nathan Road, Hong Kong, 999077, China.

3) to verify the feasibility of retrieval of the background wind velocity with the information of the characteristic size.

The paper is organized as follows. The definition of characteristic size and its impact factors are introduced in Section II. Section III presents the relationship between the characteristic size and polarimetric variables, and a new method to retrieve the characteristic size based on polarimetric variables is proposed. To better verify the performance, the proposed method is implemented to the data around the Hong Kong International Airport (HKIA) from a S-band dual-polarization Doppler weather radar in Hong Kong in Section IV, and the conclusion is drawn in Section V.

II. Definition and Factors of the Characteristic Size of Raindrops

A. Physical Features of Raindrops

In nature, a raindrop in falling is generally non-spherical due to the compression of air resistance, and the deformation for a big raindrop is typically severer than a smaller one. In the community of meteorology, oblate shape is assumed to be a good representative of the shape of a raindrop, and the equivolumetric spherical drop diameter [20] (hereafter, diameter) and axis ratio [21] (i.e., ratio of particle minor-to-major dimension) are always used to characterize the shape. According to the theory of particle's motion, a raindrop of certain diameter falls with certain terminal falling velocity in still air, which is the consequence of equilibrium between the gravity and drag force on this raindrop. According to Atlas *et al*. [22], raindrop's terminal falling velocity can be given with its diameter as

$$V_{\mathrm{T}}(D) = [\alpha_1 - \alpha_2 \exp(-\alpha_3 D)](\rho_0/\rho)^{0.4} \tag{1}$$

where D is the diameter of raindrops, $\alpha_1 = 9.65$, $\alpha_2 = 10.3$, $\alpha_3 = 0.6$, and ρ_0/ρ is ratio of the air densities in the sea surface and at the altitude of measurement. For radar detection in still air, the Doppler velocity is the projection of the terminal falling velocity on the radar beam.

It is well known that a rain case contains a lot of raindrops of different sizes, and there have been a variety of existing DSD models to characterize the size distribution, including the exponential distribution [23], gamma distribution [15] and normalized gamma distribution [16]. The exponential distribution model is given by

$$N(D) = N_0 \exp(-\Lambda D) \tag{2}$$

where N_0 is the scaling parameter and Λ is the slope parameter. The gamma distribution model is given by

$$N(D) = N_{\mathrm{m}}(D)^{\mu_{\mathrm{m}}} \exp(-\Lambda_{\mathrm{m}} D) \tag{3}$$

where N_{m} and Λ_{m} are similar to N_0 and Λ in the exponential distribution model, and μ_{m} is unitless and always fixed on 2 or 3 in most cases. The normalized gamma distribution model is given by

$$N(D) = N_{\mathrm{w}} \frac{6(3.67+\mu)^{\mu+4}}{3.67^4 \Gamma(\mu+4)} \left(\frac{D}{D_0}\right)^{\mu} \exp\left(\frac{-(3.67+\mu)D}{D_0}\right) \tag{4}$$

where N_{w} is the normalized intercept parameter, D_0 is the median volume diameter, and μ is the unitless shape parameter. Among them, the exponential distribution model was proven unsuitable for heavy rain cases [24], and the parameters of gamma distribution model are coupled to each other [25]; they are not applicable to analyze the dominant factors of the characteristic size for all different rainfall types. Comparatively, the normalized gamma distribution model is determined by independent parameters and has good adaptability to different rainfall types in nature [26]. Based on these facts, the normalized gamma distribution is adopted in this study to analyze the issues about the raindrops' characteristic size.

B. Characteristic Size of Raindrops

In a certain radar range bin, plenty of raindrops with different velocities lead to a Doppler spectrum [27], consisting of different characteristic spectral components,

$$S(v) = \sigma_{\mathrm{pol}}(D) N(D) \mid \mathrm{d}D/\mathrm{d}v \mid \tag{5}$$

where $\sigma_{\mathrm{pol}}(D)$ is the back-scattering radar cross section (RCS) of a raindrop in terms of different polarizations, $N(D)$ is the raindrop size distribution in this radar range bin, and $|\mathrm{d}D/\mathrm{d}v|$ is the Jacobean of diameter to radial velocity transformation. Here an assumption is made that a group of raindrops with a certain diameter in a radar range bin have the same velocity. In (5), the part that determines the density of the spectrum is defined as equivalent RCS σ_{e}, as shown in (6):

$$\sigma_{\mathrm{e}}(D) = \sigma_{\mathrm{pol}}(D) N(D). \tag{6}$$

If the Doppler velocity is obtained from 'hh' polarization channel (horizontal polarization for both transmission and reception), then $\sigma_{\mathrm{pol}} = \sigma_{\mathrm{hh}}$. Similarly, $\sigma_{\mathrm{pol}} = \sigma_{\mathrm{vv}}$ if the Doppler velocity is obtained from 'vv' polarization channel.

According to the definition of (5), each spectral component should correspond to a group of raindrops of a certain diameter in general. According to fluid dynamics, if the velocity and diameter for a group of raindrops are known, the motion equation for these raindrops can be established to connect the background wind velocity and the raindrops' velocity. But for a given spectral component, which diameter of raindrops' motion does this spectral component reveal? This relationship is not easy to determine.

Of course, the Doppler velocity, which is generally obtained from the strongest Doppler spectral component, also corresponds to a group of raindrops with a certain diameter. For convenience, this group of raindrops are regarded as the characteristic raindrops here, and the diameter and velocity of those raindrops are defined as characteristic size D_{c} and characteristic velocity V_{c} respectively, i.e.,

$$D_{\mathrm{c}} = \arg\max_{D} \sigma_{\mathrm{hh}}(D) N(D). \tag{7}$$

The polarization channel to obtain the Doppler spectrum is 'hh' in this paper, and the correspondence among D_{c}, V_{c} and Doppler velocity in still air is shown in Fig. 1. It is worth mentioning that the characteristic velocity is equal to the characteristic raindrops' terminal falling velocity (see Fig.

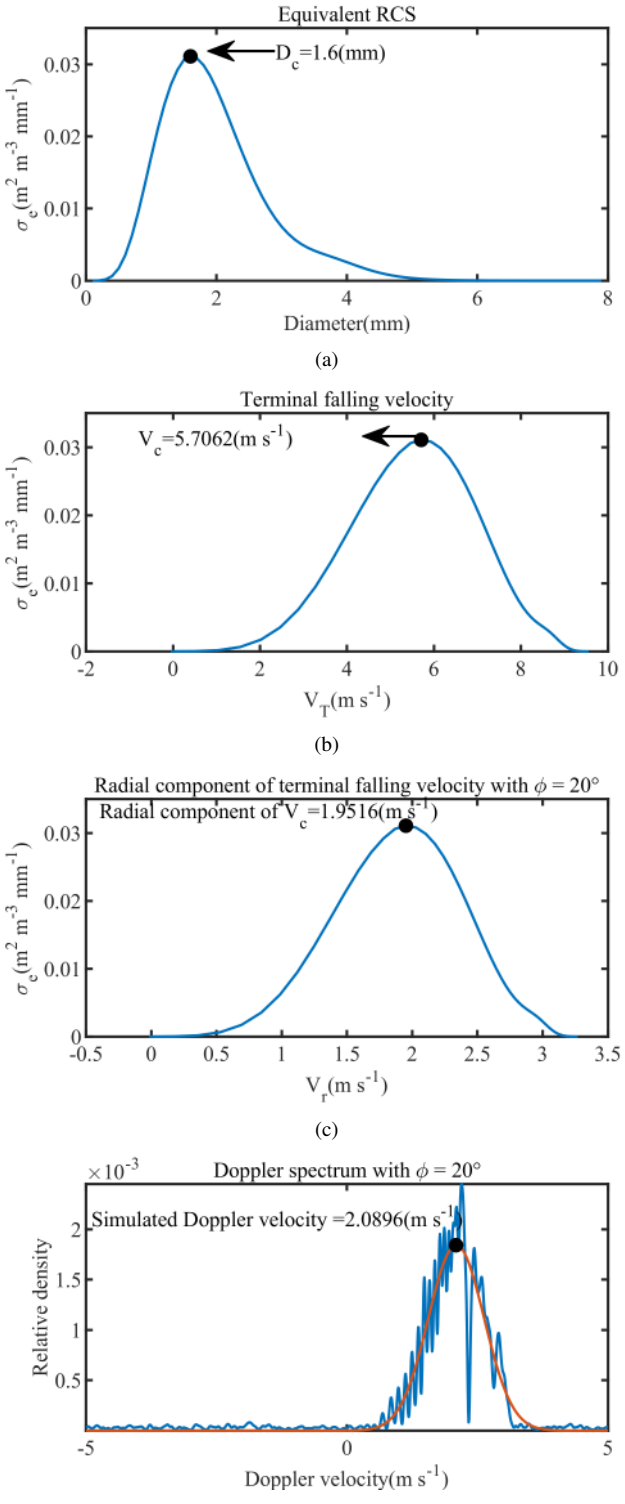

Fig. 1. Correspondence among D_{c}, V_{c} and Doppler velocity of precipitation in a certain radar range bin in still air. This figure is simulated in X-band, with $\phi = 20°$, based on normalized gamma DSD ($N_{\mathrm{w}} = 3000(\mathrm{m}^{-3} \cdot \mathrm{mm}^{-1})$, $D_0 = 1(\mathrm{mm})$, $\mu = 0$). (a) σ_{e} versus diameter. The numerical relationship between the two is shown in (7), and D_{c} corresponds to the maximum of the curve. (b) σ_{e} versus V_{T}, which is derived from curve in Fig. 1(a) with equation (1), here the velocity of a raindrop is just the raindrop's terminal falling velocity due to the hypothesis of still air. (c) σ_{e} versus V_{r}, where V_{r} is the projection of terminal falling velocity on radar beam with $\phi = 20°$. (d) Simulated Doppler spectrum, which is consistent with curve in Fig. 1(c) when noise's impact is ignorable.

1(b)) in still air, and this is useful for method's verification as discussed in Section IV.

For raindrops in a certain radar range bin, the characteristic velocity can be obtained with the Doppler velocity and radar elevation angle. Then, if the characteristic size can be determined, the motion equation of the characteristic raindrops can be established as follows [28],

$$\frac{\mathrm{d}\boldsymbol{v}}{\mathrm{d}t} = \boldsymbol{g} + \frac{g}{V_T^2}|\delta\boldsymbol{v}|\delta\boldsymbol{v}, \tag{8}$$

where $\boldsymbol{v}$ and V_{T} are the velocity and the theoretical terminal falling velocity of the characteristic raindrops respectively, g is the downward gravitational acceleration, and $\delta\boldsymbol{v}$ is the difference velocity between the background wind and the characteristic raindrops. From (8), the background wind velocity could be decoupled from the characteristic raindrops' velocity when the characteristic size is determined, as shown in Fig. 2. Thus, in this article, the main purpose is to retrieve the characteristic size, i.e., the size of raindrops corresponding to the Doppler velocity.

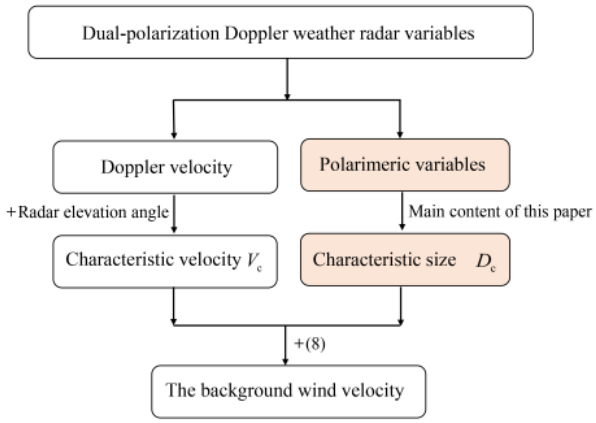

Fig. 2. Block scheme for retrieval of the background wind velocity.

C. Major Impact Factors of the Characteristic Size

As we can see in (7), the Doppler spectral density and D_{c} in a certain radar range bin are determined by both $\sigma_{\mathrm{hh}}(D)$ and $N(D)$.To retrieve D_{c} more accurately, they are studied here first.

1) Scattering Property of Raindrops: In general, the RCS of a non-spherical raindrop is determined by the radar wavelength (λ), elevation angle (ϕ), and the orientation of this raindrop. T-matrix method [29], which is a good RCS simulation toolbox for ellipsoid target, can be used to simulate the RCS of a raindrop in terms of different parameters, for example, radar wavelength, elevation angle and raindrop's orientation.

S/C/X band radars are widely used for remote sensing in precipitation [30], so we take 3 representative wavelengths as examples (111mm for S-band, 53.5mm for C-band and 33.3mm for X-band) to study the impact of wavelength on the RCS of a raindrop. Because the horizontal incidence wave ($\phi = 0°$) cannot detect the terminal falling velocity of raindrops and the vertical incidence case ($\phi = 90°$) is not

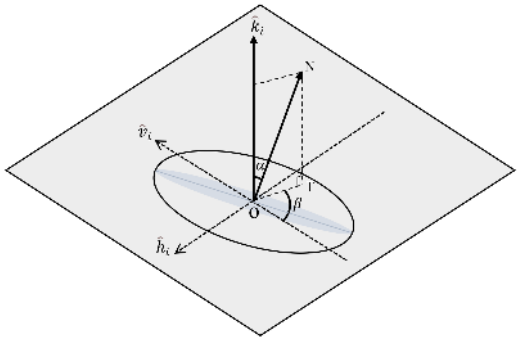

Fig. 3. Raindrop's orientation. $\widehat{h_i}/\widehat{v_i}$ is the orientation of horizontal/vertical polarization and $\widehat{k_i}$ is the orientation of the incidence wave. $\overline{ON}$ is the symmetry axis of this raindrop, and $\overline{OT}$ is the projection of the symmetry axis on the plane of polarization. α and β are always used to express the orientation of the raindrop.

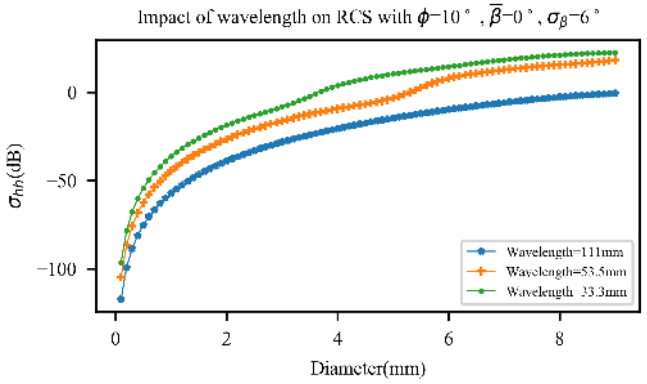

(a)

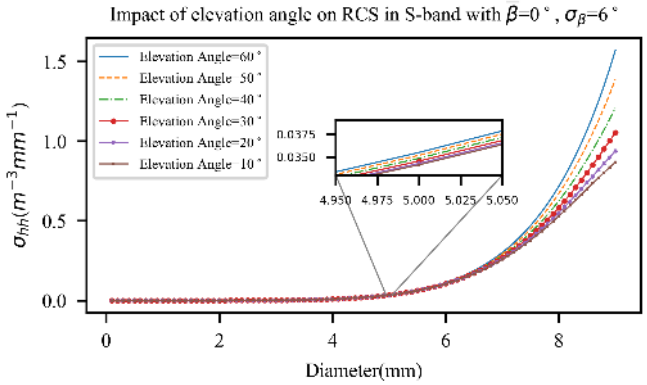

(b)

Fig. 4. The major impact factors for the RCS of a single raindrop. (a) The impact of radar wavelengths on the RCS. The elevation angle is 10°, and the canting angle is set to be a Gaussian distribution with zero mean and standard deviation of 6°. (b) The impact of elevation angles on the RCS. The wavelength is 111mm and the canting angle is set to be a Gaussian distribution with zero mean and standard deviation of 6°.

sensitive to polarimetric information of raindrops, the elevation angles in this study are set in range between 10° to 60°, at a step of 10°. A raindrop's orientation can generally be determined by two angles α and β (see Fig. 3), where α is the angle between the incidence direction and the symmetry axis of this raindrop, and β, called the canting angle, is the angle between the vertical direction on the plane of polarization and the drop's symmetry axis on the same plane. Generally, α is assumed to obey the uniform distribution in [0°, 360°], and β can be approximated with a Gaussian distribution with zero mean and small standard deviation (6° in low wind conditions and 12° in moderate wind conditions typically, and rarely smaller than 1° or larger than 21°) [31], [32]. Given that the orientation of raindrops cannot be determined in advance, we only compared the scattering properties for different radar wavelengths and elevation angles in this part.

As shown in Fig. 4(a), the RCS curves for different wavelengths are different from each other. Similarly, the impact of elevation angles is also visible in Fig. 4(b), especially for bigger raindrops whose shape deformations are severer. Besides, bigger raindrops always have bigger RCS, so the equivalent RCS σ_e should present a more special distribution if a DSD includes more big raindrops.

2) DSD of Raindrops and Its Impact on D_c: As shown in (4), the normalized gamma DSD is determined by parameters N_w, D_0 and μ. In this analysis, the parameter N_w is fixed as $N_w = 3000$ since it does not influence the characteristic size D_c, and we try to find out the dependence of D_c on D_0 and μ. Here D_0 varies in [1.75, 3] and μ varies in [9, 20] with 5 linearly distributed samples. Part of the simulation results for the concerned S-band radar at $\phi = 10°$, $\overline{\beta} = 0°$ and $\sigma_\beta = 6°$ are shown in Fig. 5. It's can be observed that the value of D_c increases with the increase of D_0 and the decrease of μ. Thus, a potential way to obtain D_c with existing methods is to retrieve D_0 and μ first, and then calculate D_c with the retrieved results. During this process, the retrieval of D_0 and μ is the average effect of a lot of observations, and the error accumulation always happens when D_c is obtained from the averaged parameters. To avoid the unnecessary errors, this study aims to propose a new method to retrieve D_c directly from observed polarimetric variables.

III. The Method to Retrieve the Characteristic Size

As discussed in Section II, D_c is mainly influenced by 5 parameters, say, the radar band, elevation angle, canting angle, the median volume diameter and the shape parameter of DSD. In radar detection campaigns, only the radar frequency and observing elevation angle are known in advance, so this study aims to retrieve D_c from the radar observing data in terms of different orientation distribution and size distribution of raindrops. Here, the radar in use is assumed to be a dual-polarization radar due to its good ability in characterizing the size and shape of raindrops over large spatial and temporal scales.

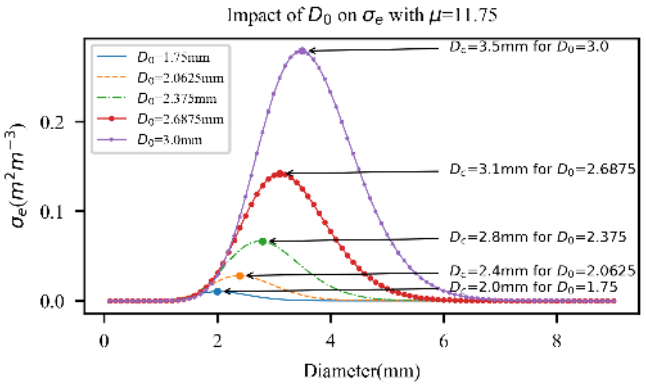

(a)

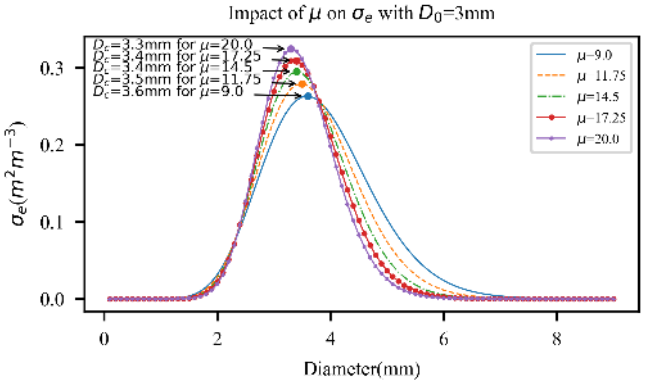

(b)

Fig. 5. The impact of normalized gamma DSD parameters on equivalent RCS and raindrops' characteristic size. (a) The impact of D_0. The radar band is S-band, and elevation angle is 10°, the canting angle is set to be a Gaussian distribution with zero mean and standard deviation of 6°, and μ is 11. The characteristic size increases with the increase of D_0. (b) The impact of μ. D_0 is 3mm and the characteristic size decreases with the increase of μ when the other parameters are the same with Fig. 4(a).

A. The Relationship Between Polarimetric Variables and Characteristic Size of Raindrops

The polarimetric variables provided by a dual-polarization Doppler weather radar include the radar reflectivity $Z_{\rm h}$ and $Z_{\rm v}$, differential reflectivity $Z_{\rm dr}$, specific differential phase $K_{\rm DP}$, differential phase shift $\Phi_{\rm DP}$, copolar correlation coefficient $\rho_{\rm hv}$ and linear depolarization ratio $L_{\rm dr}$, and $Z_{\rm H}$/$Z_{\rm DR}$/$L_{\rm DR}$ mean the value of $Z_{\rm h}$/$Z_{\rm dr}$/$L_{\rm dr}$ in logarithmic scale [33]. Among them, $Z_{\rm dr}$ and $K_{\rm DP}$ are strongly related to the shape/size of raindrops, but the big influence of canting angle on these two variables may degenerate their ability for representing the shape/size. However, the circular depolarization ratio $C_{\rm dr}$, which mainly depends on the raindrops' shape, is insensitive to the orientations of raindrops. Even though $C_{\rm dr}$ has such a good property, it is not easy to be obtained directly from a linear polarization radar. Fortunately, the depolarization ratio $D_{\rm r}$ shown in (9) can serve as a proxy for it, and the impact of propagation effect on $D_{\rm r}$ is almost negligible from low frequency radars [34]–[39]. So, in this study, $D_{\rm r}$ is taken as a key variable to retrieve $D_{\rm c}$, and $D_{\rm R}$ denotes the value of $D_{\rm r}$ in logarithmic scale.

$$D_{\rm r}=\frac{1+Z_{\rm dr}^{-1}-2\rho_{\rm hv}Z_{\rm dr}^{-1/2}}{1+Z_{\rm dr}^{-1}+2\rho_{\rm hv}Z_{\rm dr}^{-1/2}} \tag{9}$$

Simulations based on T-matrix were carried out to show the relationships between the above polarimetric variables ($Z_{\rm H}$, $Z_{\rm DR}$, $K_{\rm DP}$, $\rho_{\rm hv}$, $L_{\rm DR}$, $D_{\rm R}$) and $D_{\rm c}$ in terms of different radar and rain parameters shown in Table I [15], where the normalized gamma DSD was adopted. It's worth noticing that $N_{\rm w}$ is set to vary in (1,000, 100,000) with 9 linearly distributed samples in this part, because $N_{\rm w}$ can also influence the polarimetric variables.

TABLE I
PARAMETER SET OF RADAR AND RAINDROPS

Parameter type	Values
Radar wavelength λ	111mm(S-band) 53.5mm(C-band) 33.3mm(X-band)
Elevation angle ϕ	10°,20°,30°,40°,50°,60°
Mean canting angle $\overline{\beta}$	0°,1°,2°
Standard deviation of $\beta(\sigma_\beta)$	1°,3°,6°,9°,12°,15°,18°,21°
Normalized intercept parameter $N_{\rm w}(\rm m^{-3}\cdot mm^{-1})$	9 linearly distributed samples in (1,000, 100,000)
Median diameter $D_0(\rm mm)$	9 linearly distributed samples in (0.5, 3.0)
Shape parameter μ	9 linearly distributed samples in (-2, 20)

We first take S-band as an example to show the dependency of characteristic size on different polarimetric variables ($Z_{\rm H}$, $Z_{\rm DR}$, $K_{\rm DP}$, $\rho_{\rm hv}$, $L_{\rm DR}$, $D_{\rm R}$), and the simulation results are shown in Fig. 6. In each subfigure, a group of data for a marker are with a certain elevation angle (ϕ), but different settings of canting angles ($\overline{\beta}$, σ_β) and DSD parameters ($N_{\rm w}$, D_0, μ). It's obvious that $Z_{\rm H}$, $K_{\rm DP}$ and $L_{\rm DR}$ are not good proxies for $D_{\rm c}$ because one value of $Z_{\rm H}$/$K_{\rm DP}$/$L_{\rm DR}$ may correspond to two or more very different values of $D_{\rm c}$. The copolar correlation coefficient $\rho_{\rm hv}$ almost does not change in the whole range of $D_{\rm c}$, so it is not a good proxy for the characteristic size $D_{\rm c}$, either.

For the rest two polarimetric variables $Z_{\rm DR}$ and $D_{\rm R}$, they are strongly related to the elevation angle, but fortunately, the elevation angle is generally known in advance. When attention is paid to a certain elevation angle, both $Z_{\rm DR}$ and $D_{\rm R}$ have a functional relationship with $D_{\rm c}$, in detail, an approximately linear relationship for $Z_{\rm DR}\sim D_{\rm c}$ and an approximately exponential relationship for $D_{\rm R}\sim D_{\rm c}$. In terms of that, $Z_{\rm DR}$ seems to be a better choice than $D_{\rm R}$ because a linear relationship generally leads to a smaller fitting error than an exponential relationship. However, for all the elevation angles, the variation of $Z_{\rm DR}$ depending on canting angles is always much more noticeable than that of $D_{\rm R}$. Furthermore, the canting angle's impact on $Z_{\rm DR}$ gets severer as the radar beam gets more slant from the zenith, but that impact on $D_{\rm R}$ is almost negligible when the elevation angle is around 45°. From this point of view, both $Z_{\rm DR}$ and $D_{\rm R}$ have their advantages and disadvantages in determining $D_{\rm c}$. If the advantages of the two variables can be integrated, better estimation of $D_{\rm c}$ might be

This article has been accepted for publication in a future issue of this journal, but has not been fully edited. Content may change prior to final publication. Citation information: DOI 10.1109/JSTARS.2021.3113651, IEEE Journal of Selected Topics in Applied Earth Observations and Remote Sensing

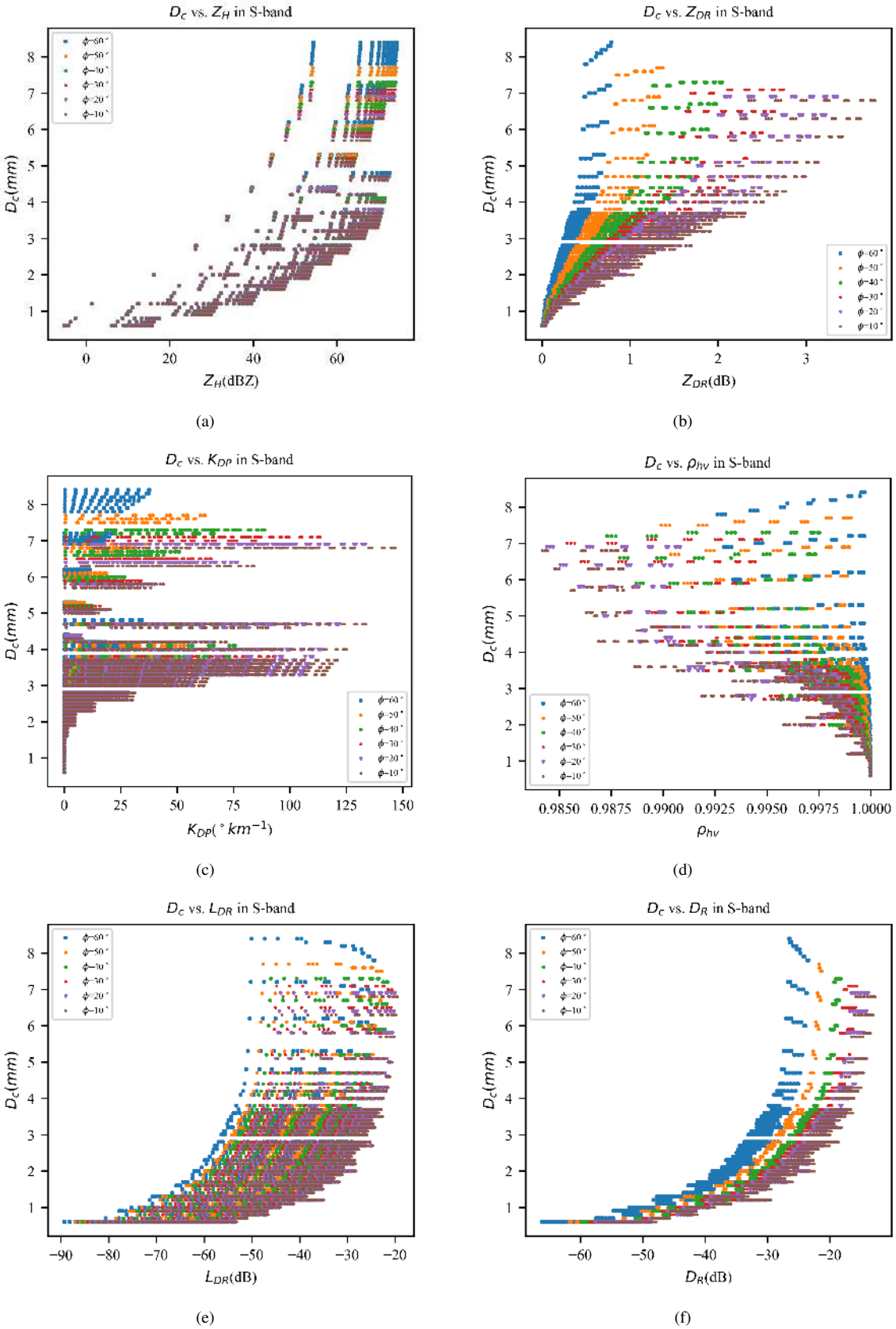

Fig. 6. Relationship between polarimetric variables and D_c in S-band. (a) D_c versus Z_H. (b) D_c versus Z_{DR}. (c) D_c versus K_{DP}. (d) D_c versus ρ_{hv}. (e) D_c versus L_{DR}. (f) D_c versus D_R.

expected, which has been substantiated by simulation results (part B in this section) and radar measurements (Section IV).

B. The Retrieval Model and Evaluation

In order to find the best proxy for D_{c}, retrieval models based on Z_{DR}, D_{R} and $Z_{\mathrm{DR}} + D_{\mathrm{R}}$ need to be established respectively, in other words, optimal functions for $D_{\mathrm{c}} = f_1(Z_{\mathrm{DR}})$, $D_{\mathrm{c}} = f_2(D_{\mathrm{R}})$ and $D_{\mathrm{c}} = f_3(Z_{\mathrm{DR}}, D_{\mathrm{R}})$ need to be found in this part. As discussed in Section II and shown in Fig. 6, the relationship between $Z_{\mathrm{DR}}/D_{\mathrm{R}}$ and D_{c} changes a lot among different radar bands and elevation angles, so it's better to analyze data for each radar band and elevation angle. It is a fundamental regression issue to establish a retrieval model of D_{c} from $Z_{\mathrm{DR}}/D_{\mathrm{R}}$, and a common tool to deal with that is support vector regression (SVR), which is a derivation of support vector machine (SVM) with good robustness and efficiency [40]–[42]. The basic idea of SVR is to convert the nonlinear regression in sample space to linear regression in higher-dimensional space (feature space) by using kernel functions, and the common kernel functions include linear kernel function and radial basis function (RBF), the former is mainly suitable for linear regression issues and the later can be used in both linear and nonlinear regression issues [43], [44]. In this study, the relationship between D_{R} and D_{c} is obviously not linear relationship, so the RBF kernel function is chosen due to its excellent adaptability.

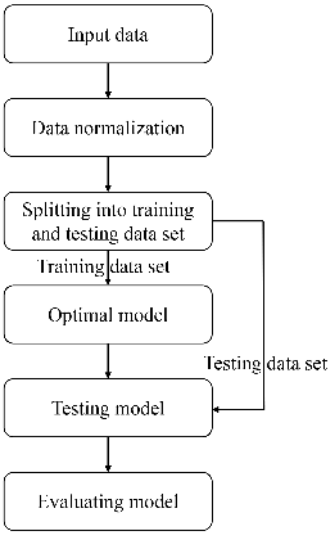

Fig. 7. The flow chart to build and evaluate the retrieval models.

The flow chart to build and evaluate the retrieval models based on simulation data is shown in Fig. 7. First, for each radar band and elevation angle shown in Table I, simulations were carried out to obtain data set as the input data ($Z_{\mathrm{DR}} \sim D_{\mathrm{c}}$, $D_{\mathrm{R}} \sim D_{\mathrm{c}}$, and $'Z_{\mathrm{DR}} + D'_{\mathrm{R}} \sim D_{\mathrm{c}}$). According to existing studies, raindrop size distribution varies for different regions [45], [46]. Besides the normalized gamma DSD shown in part A of this section, exponential DSD and gamma DSD for rain cases in a specific region were also taken into account in this part to enrich the experiment results, and the parameters of the two DSDs can be found in Table III in Sumbiri et al. [46]. The next step is data preprocessing, i.e., normalizing the input data and dividing them into training data set (accounting for 80%) and testing data set (accounting for 20%). Then the training data set was used to establish the optimal model based on SVR, and the testing data set was used to evaluate that model.

Part of the retrieval models for concerned S-band are shown in Fig. 8. Fig. 8(a) shows the retrieval models based on Z_{DR} for different elevation angles, where different markers mean samples for different elevation angles, and the curves surrounded by each kind of markers are the predicted results with testing data set and show the tendency of corresponding retrieval models. It is worth noting that the retrieval model for each elevation angle seems to be off the center of the samples, which is because the samples are denser at the location of the curve, as we can see in the zoom figure in Fig. 8(b). Fig. 8(c) shows the retrieval models based on D_{R} for different elevation angles. It is observed that the SVR results for D_{R} are obviously better than the Z_{DR} related models due to the less diversity of the Z_{DR} related simulation results. The relationship between fusion result and $Z_{\mathrm{DR}}/D_{\mathrm{R}}$ should be a 3D-surface for each elevation angle. For simplicity, here we only show the retrieval model based on $Z_{\mathrm{DR}}+D_{\mathrm{R}}$ for $\phi = 10^\circ$ in S-band (see Fig. 8(d)), where the triangle-down markers ($\bigtriangledown$) mean the training data set and the point markers ($\cdot$) mean the predicted data with testing data set.

Even though the predicted data seem to comply well with the training data set in Fig. 8, the retrieval errors are not intuitive, especially for the fusion models. In this article, root mean square error (RMSE) is used to characterize the performance of the estimation,

$$\mathrm{RMSE} = \sqrt{\frac{1}{N}\sum_{i=1}^{N}(y_i - \widehat{y_i})^2}(\mathrm{mm}) \tag{10}$$

where N is the number of parameters in the testing data set, y_i is the true value of D_{c} for the i-th sample in the testing data set, $\widehat{y_i}$ is an estimation of y_i. Generally speaking, a smaller RMSE means a better retrieval model. Here, process to build and evaluate the retrieval model for each input data was repeated for 5 times because the procedure to divide the input data set into training data and testing data is stochastic to some extent, and the averaged evaluation results are shown in Fig. 9.

In Fig. 9, different markers represent different DSD models. In detail, point markers ($\cdot$) and triangle-down markers ($\bigtriangledown$) are related to the exponential DSD and gamma DSD, respectively, and star markers ($\star$) are related to the normalized gamma DSD. On the whole, compared with those from the normalized gamma DSD, models based on data set derived from the exponential DSD and gamma DSD for a specific region perform better. The reason of this phenomenon is that the precipitation cases described by the normalized gamma DSD are more universal, while the other two DSDs mainly describe cases limited to a specific region. Therefore, the prior information of DSD model type for a specific region is useful to improve the performance of the retrieval models.

For retrieval models based on Z_{DR}, shown by solid lines in Fig. 9, the RMSE increases with the increase of elevation an-

This article has been accepted for publication in a future issue of this journal, but has not been fully edited. Content may change prior to final publication. Citation information: DOI 10.1109/JSTARS.2021.3113651, IEEE Journal of Selected Topics in Applied Earth Observations and Remote Sensing

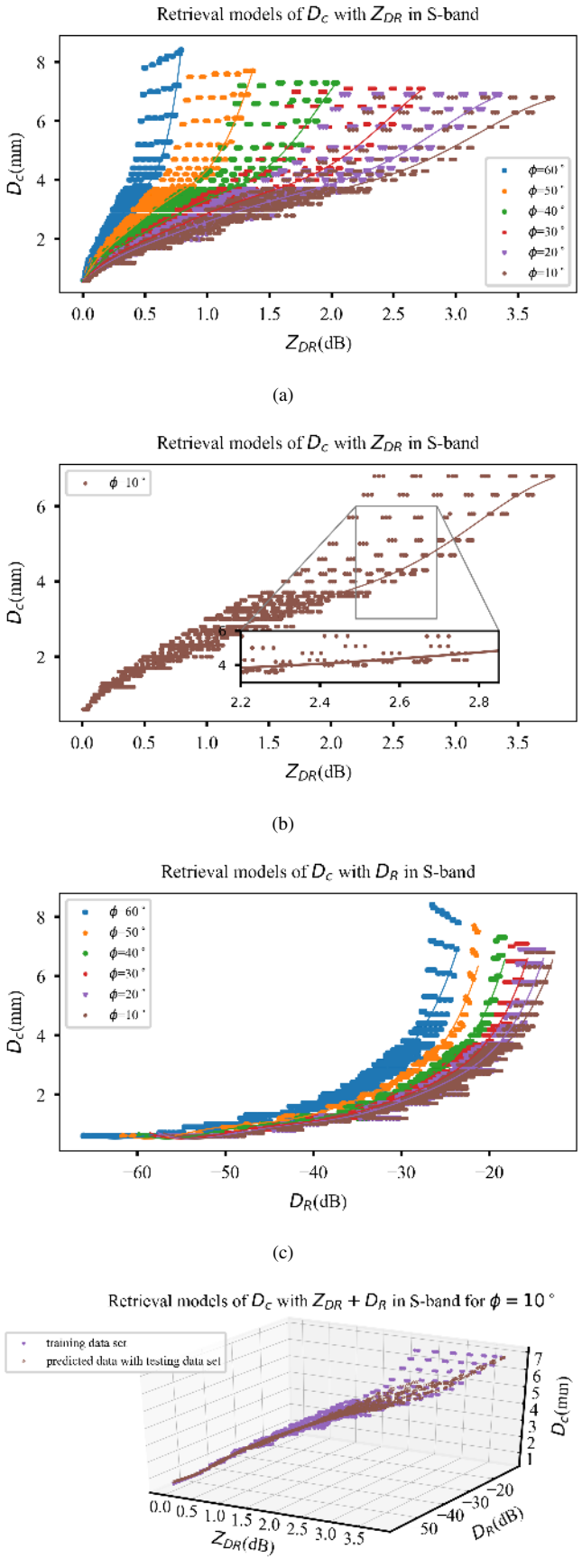

Fig. 8. The retrieval models in S-band. (a) The retrieval models based on Z_{DR} for different elevation angles. (b) The retrieval models based on Z_{DR} for $\phi = 10°$. (c) The retrieval models based on D_{R} for different elevation angles. (d) The retrieval model based on $Z_{\mathrm{DR}} + D_{\mathrm{R}}$ for $\phi = 10°$.

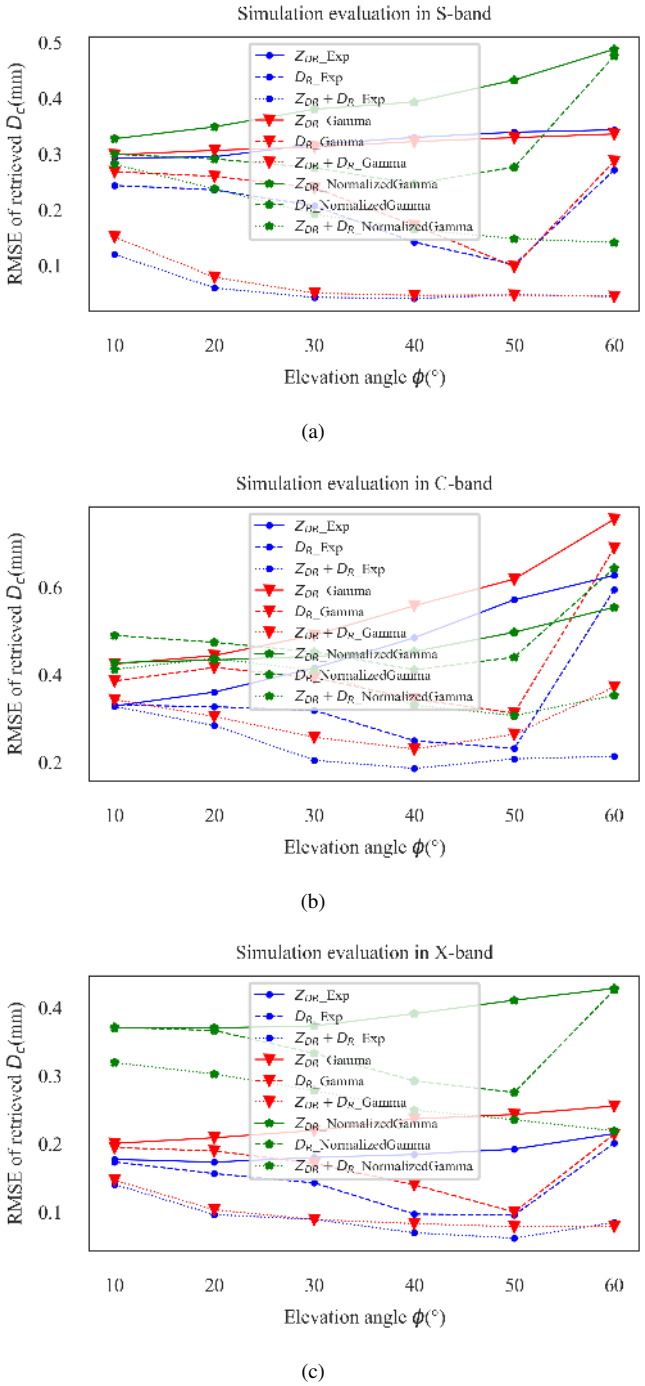

Fig. 9. The evaluation results of retrieval models. (a) RMSE of retrieval models in S-band. (b) RMSE of retrieval models in C-band. (c) RMSE of retrieval models in X-band.

gles, which is mainly caused by the smaller gradients of Z_{DR} for larger elevation angles. For retrieval models based on D_{R}, shown by dashed lines in Fig. 9, it is clear that the retrieval quality reaches the best when elevation angle is around $45°$. This is caused by the fact that the data around $45°$ are more gathering than those in the rest angles. Therefore, elevation angles around $45°$ are suggested for retrieval models based on D_{R} . By comparing the evaluation results of retrieval models based on Z_{DR} and D_{R}, models based on D_{R} perform better in most cases. Furthermore, better performance is expected with the fusion models combining both Z_{DR} and D_{R}, which is actually indicated by the dotted lines in Fig. 9.

IV. Method Verification with Field Observation Data

To better show the performance of the retrieval method proposed in Section III, verification of it with field observation data (radar data and disdrometer data) has been carried out. The radar data around Hong Kong International Airport (HKIA) was collected with a S-band dual linear polarization Doppler weather radar. The elevation angles for observation were $10°$, $22°$ and $34°$, and the product data include Z_{DR}, ρ_{hv} and Doppler velocity. The disdrometer data was collected with a 2D video disdrometer, which was located at an azimuth of $260°$ and 31 km away from the radar, as shown by the star marker ($\star$) in Fig. 10.

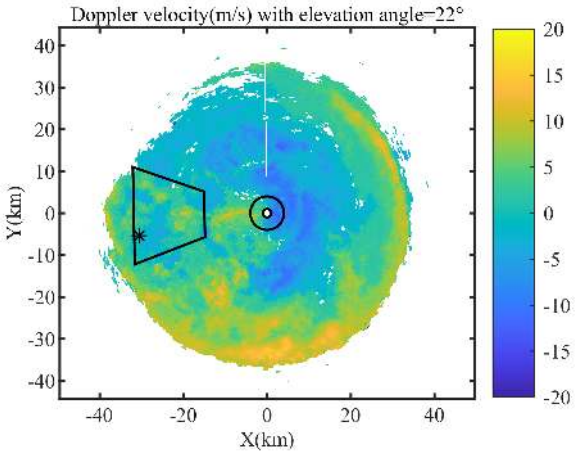

Fig. 10. The Doppler velocity of PPI scan around 12:21 UTC on 30 September 2020 with elevation angle=22°.The center of this figure is the location of radar and the star marker indicates the location of the disdrometer. The region enclosed by the quadrilateral is where the polarimetric data is selected, while the region between the two rings is where the Doppler velocity data is selected.

A. Verification of the Retrieved Characteristic Size

As said above, the polarimetric variables of radar data can be used to retrieve the raindrops' characteristic size. And the DSD obtained from the disdrometer can also be used to directly calculate D_{c} with the scattering property of raindrops, which can be treated as the benchmark to evaluate D_{c} retrieved from the radar data. On 30 September 2020, 4 May 2021 and 1 June 2021, rain cases were detected by the disdrometer and radar, and the data set are used to verify the proposed method. With the disdrometer data, the raindrop size distribution can be computed with [47]

$$N(D_i) = \frac{1}{\Delta T \Delta D} \sum_{j=1} \frac{1}{A_j v_j} (\mathrm{m}^{-3} \cdot \mathrm{mm}^{-1}) \qquad (11)$$

where D_i is the diameter of category i, ΔT is the integration time (300 seconds in this study), ΔD is the width of the size class (0.1mm in this study), A_j is the disdrometer effective measurement area during the collection of drop j, and v_j is the falling velocity of raindrop j. According to the radar scanning frequency, the time frame was set with an interval of 6 minutes. Then the equivalent RCS at each time frame can be computed with (6), which can be fitted to a Gaussian curve to get an estimation of D_{c} with (7). The equivalent RCS around 12:21 UTC on 30 September 2020 is shown in Fig. 11.

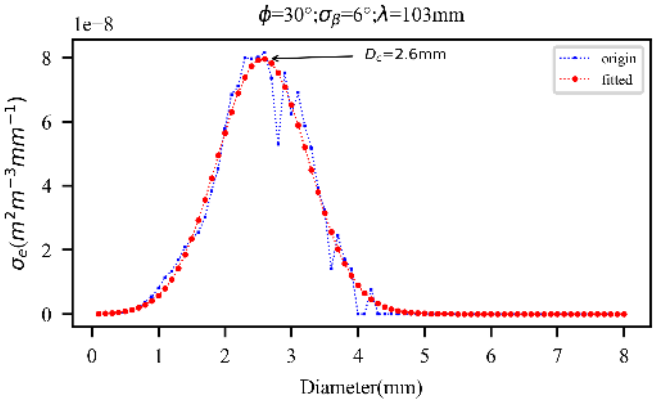

Fig. 11. σ_{e} and D_{c} calculated with $\phi = 30°$, $\sigma_\beta = 6°$ and $\lambda = 103$mm around 12:21 UTC on 30 September 2020. The result is averaged in 5 minutes. The blue line is the original σ_{e} calculated with (6) and the red line is the Gaussian curve fit of the data.

TABLE II
RMSE of Retrieved D_{c} for Three Rain Cases

No.	ϕ	RMSE($D_{\mathrm{c}}^{Z_{\mathrm{DR}}}$)	RMSE($D_{\mathrm{c}}^{D_{\mathrm{R}}}$)	RMSE($D_{\mathrm{c}}^{Z_{\mathrm{DR}}+D_{\mathrm{R}}}$)
1	10°	0.7901	0.7514	0.6066
	22°	0.7021	0.6645	0.5505
	34°	0.9714	0.8823	0.5924
2	10°	0.9057	0.8962	0.7282
	22°	0.8228	0.8312	0.7184
	34°	1.2257	1.1203	0.8156
3	10°	0.5677	0.5360	0.4454
	22°	0.8732	0.7941	0.4989
	34°	1.3050	1.1302	0.6567
average		0.9071	0.8451	**0.6236**

Considering the relative location of radar and disdrometer, the radar data of azimuth in range from $250°$ to $290°$ and radial distance from 16 km to 34 km were selected here to guarantee the correlation of data from different instruments, as shown by the quadrilateral in Fig. 10. After basic quality control of the data (for example, Z_{DR} is limited in [0.5, 3] which is a value range of Z_{DR} in previous studies [33], [34], [48] and in our simulation), D_{R} was calculated with Z_{DR} and

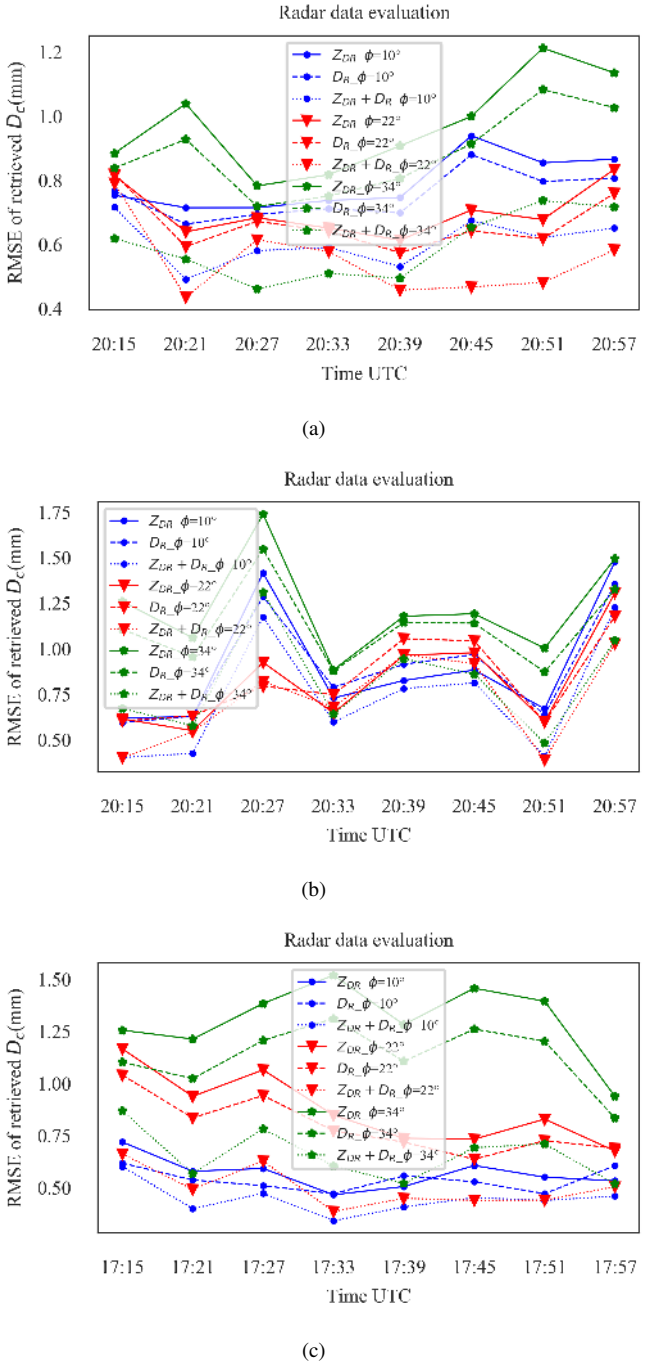

Fig. 12. RMSE of retrieved D_c for different retrieval models, where the radar data come from a S-band dual-polarization radar and the benchmark is D_c calculated with disdrometer data.(a) Model evaluation with data detected on 30 September 2020. (b) Model evaluation with data detected on 4 May 2021. (c) Model evaluation with data detected on 1 June 2021.

ρ_{hv} by (9), then Z_{DR} and D_R of different elevation angles were input to the SVR model trained by simulation data in Section III. During the process of comparison and verification, one kind of characteristic size $D_c^{\text{Disdrometer}}$ can be obtained by combining the disdrometer data and the scattering property of raindrops, and other three kinds of characteristic size, i.e., $D_c^{Z_{DR}}$, $D_c^{D_R}$ and $D_c^{Z_{DR}+D_R}$, can be obtained from the retrieval models based on Z_{DR}, D_R and the fusion models of $Z_{DR} + D_R$, respectively. For a certain elevation angle at each time frame, the RMSE of retrieved D_c is shown in Fig. 12, where the benchmark is $D_c^{\text{Disdrometer}}$ obtained from the disdrometer data, the solid/dashed lines mean the RMSE of D_c retrieved with models based on Z_{DR}/D_R, and the dotted lines mean the RMSE of D_c retrieved with the fusion models. To make it clearer, RMSE of retrieved D_c from radar data is shown in Table II, where the data corresponding to each ϕ in each case is the averaged value for time frames. It is obvious that the fusion models combining the information of Z_{DR} and D_R always perform better for all the three cases; this phenomenon meets well with the conclusion of simulation results in Section III.

B. Verification of the Velocity of the Characteristic Raindrops

The main purpose of this study is to retrieve D_c and analyze the interaction between raindrops and the background wind, which can provide basic model support to retrieve the background wind velocity in the further study. As we can see in (8), if the background wind field is comparatively stable, the horizontal velocity component of the characteristic raindrops should be identical to that of the background wind, while the velocity difference between the characteristic raindrops and the background wind in vertical orientation should be equal to the terminal falling velocity of the characteristic raindrops (V_T), i.e.,

$$\delta v_z = v_z^{D_c} - v_z^b = V_T^{D_c} \tag{12}$$

where $v_z^{D_c}$ is the vertical velocity component of the characteristic raindrops, v_z^b is that component of the background wind velocity , and $V_T^{D_c}$ is the terminal falling velocity of the characteristic raindrops (see (1)). In other words, $v_z^{D_c}$ should be equal to the sum of v_z^b and $V_T^{D_c}$, and this relationship can be used to evaluate the retrieval models of D_c proposed in Section III. Theoretically, we need to know v_z^b when we evaluate the D_c retrieval models based on (12), however, due to the limited experimental conditions, we did not have any anemometer to detect v_z^b at high altitude (this problem may be solved by using UAV (unmanned aerial vehicle) based anemometer [49] in our further work). So, we chose the radar data under comparatively stable air condition for velocity verification, where v_z^b is approximately equal to zero.

With the Doppler velocity detected by radar, the vertical velocity component of the raindrops can be obtained with VAD (velocity-azimuth display) method if the background wind obeys a linear distribution model [50]. For a certain radar range bin at azimuth angle θ and elevation angle ϕ, the Doppler velocity can be written as [11]

$$v_D = u\cos\theta\cos\phi + v\sin\theta\cos\phi + w\sin\phi, \tag{13}$$

where u and v are the horizontal components and w is the vertical component of the characteristic raindrops' velocity. For a certain region, the characteristic raindrops' velocity can be seen as a constant when assuming a uniform wind field. Then for a specific elevation angle, there should be a trigonometric function relationship between v_{D} and θ, i.e.,

$$v_{\mathrm{D}} = \sqrt{u^2+v^2}\cos\phi\sin(\theta+\theta_0) + w\sin\phi \qquad (14)$$

where $\theta_0 = \sin^{-1}\left(u/\sqrt{u^2+v^2}\right)$. After data quality control (for example, removing abnormal v_{D} with 3-Sigma method, i.e., calculating mean value $\overline{x}$ and standard deviation σ_x of samples, and outlier beyond $[\overline{x}-3\sigma_x, \overline{x}+3\sigma_x]$ is removed), the observation data can be fitted to a trigonometric function to obtain the three components of the characteristic raindrops' velocity, i.e., u, v and w, and w is just $v_{\mathrm{z}}^{D_{\mathrm{c}}}$ said above. Fig. 13 presents 3 groups of data and fit curves, and the good agreement between the observation data and the triangular fit curves confirms the stable air condition in selected region.

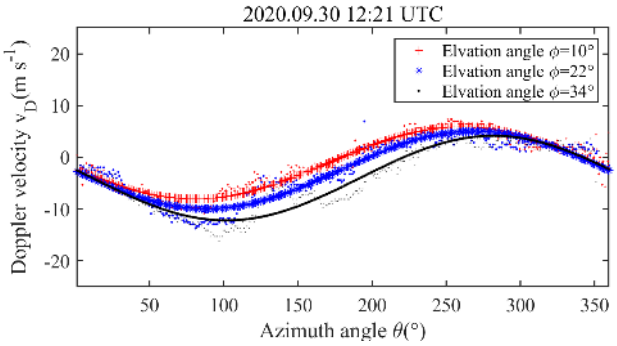

Fig. 13. Relationship between v_{D} and θ. This figure comes from the radar data around 12:21 UTC on 30 September 2020 with different elevation angles, and the radial distance is 1 km.

Fig. 14 shows the comparison results of velocities retrieved with different methods around 12:21 UTC on 30 September 2020. In the figure, the solid lines mean the terminal falling velocity of $D_{\mathrm{c}}^{\mathrm{Disdrometer}}$, the dashed lines mean $v_{\mathrm{z}}^{D_{\mathrm{c}}}$ derived from the Doppler velocity with VAD method, the three histograms in each subplot represent the terminal falling velocity distribution of $D_{\mathrm{c}}^{Z_{\mathrm{DR}}}$, $D_{\mathrm{c}}^{D_{\mathrm{R}}}$ and $D_{\mathrm{c}}^{Z_{\mathrm{DR}}+D_{\mathrm{R}}}$ respectively. The solid curves are the fit curves of those histograms, and the maximum of each curve is marked by the dash-dotted line. The RMSE of retrieved terminal falling velocities for different characteristic sizes ($D_{\mathrm{c}}^{Z_{\mathrm{DR}}}$, $D_{\mathrm{c}}^{D_{\mathrm{R}}}$, $D_{\mathrm{c}}^{Z_{\mathrm{DR}}+D_{\mathrm{R}}}$) with different benchmarks ($V_{\mathrm{T}}(D_{\mathrm{c}}^{\mathrm{Disdrometer}})$ and $v_{\mathrm{z}}^{D_{\mathrm{c}}}$(Doppler)) are shown in Table III and Table IV. Two phenomena found in Fig. 14, Table III and Table IV are as follows.

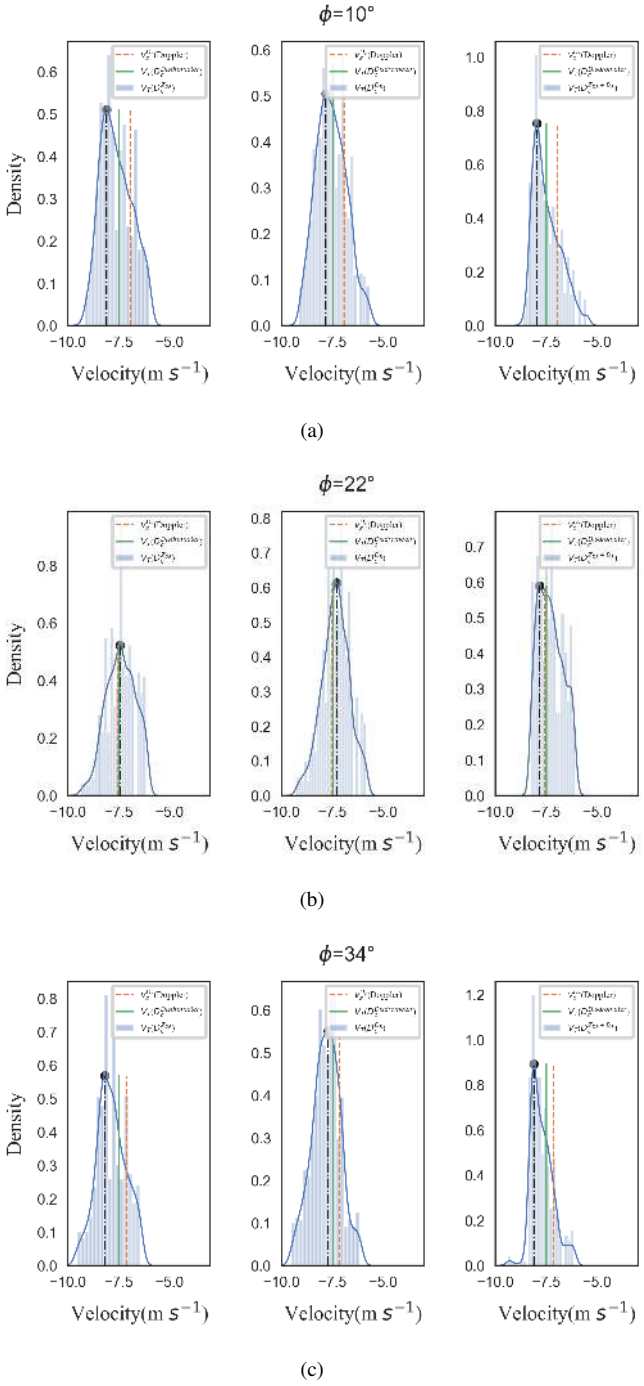

Fig. 14. The comparison results of velocities retrieved with different methods around 12:21 UTC on 30 September 2020. (a) The comparison result for $\phi = 10°$. (b) The comparison result for $\phi = 22°$. (c) The comparison result for $\phi = 34°$.

TABLE III
RMSE OF RETRIEVED VELOCITIES WHEN THE BENCHMARK IS $V_{\mathrm{T}}(D_{\mathrm{c}}^{\mathrm{Disdrometer}})$

RMSE / ϕ	$V_{\mathrm{T}}(D_{\mathrm{c}}^{Z_{\mathrm{DR}}})$	$V_{\mathrm{T}}(D_{\mathrm{c}}^{D_{\mathrm{R}}})$	$V_{\mathrm{T}}(D_{\mathrm{c}}^{Z_{\mathrm{DR}}+D_{\mathrm{R}}})$
10°	0.77	0.74	0.67
22°	0.72	0.70	0.63
34°	0.81	0.76	0.59

TABLE IV
RMSE OF RETRIEVED VELOCITIES WHEN THE BENCHMARK IS $v_{\mathrm{z}}^{D_{\mathrm{c}}}$(DOPPLER)

RMSE / ϕ	$V_{\mathrm{T}}(D_{\mathrm{c}}^{Z_{\mathrm{DR}}})$	$V_{\mathrm{T}}(D_{\mathrm{c}}^{D_{\mathrm{R}}})$	$V_{\mathrm{T}}(D_{\mathrm{c}}^{Z_{\mathrm{DR}}+D_{\mathrm{R}}})$
10°	1.02	0.95	0.85
22°	0.73	0.71	0.66
34°	1.02	0.96	0.78

First, good agreement between $V_{\mathrm{T}}(D_{\mathrm{c}}^{\mathrm{Disdrometer}})$ and $v_{\mathrm{z}}^{D_{\mathrm{c}}}$(Doppler) indicates that the velocity of the characteristic raindrops determined by the equivalent RCS is a potential proxy of the Doppler velocity of that group of raindrops. Besides, the difference between $V_{\mathrm{T}}(D_{\mathrm{c}}^{\mathrm{Disdrometer}})$ and $v_{\mathrm{z}}^{D_{\mathrm{c}}}$(Doppler) might be caused by two factors: ① errors from the velocity retrieval method VAD and ② the vertical component $v_{\mathrm{z}}^{\mathrm{b}}$ of the background wind is approximately set as zero. If $v_{\mathrm{z}}^{\mathrm{b}}$ can be measured by an instrument in the experiment, better agreement between $v_{\mathrm{z}}^{D_{\mathrm{c}}}$(Doppler) and $v_{\mathrm{z}}^{\mathrm{b}} + V_{\mathrm{T}}(D_{\mathrm{c}}^{\mathrm{Disdrometer}})$ is expected.

Second, based on the comparison of RMSE, we can see that the terminal falling velocity corresponding to the characteristic size ($D_{\mathrm{c}}^{Z_{\mathrm{DR}}}$, $D_{\mathrm{c}}^{D_{\mathrm{R}}}$, $D_{\mathrm{c}}^{Z_{\mathrm{DR}}+D_{\mathrm{R}}}$) obtained from polarimetric variables is almost equal to the vertical component $v_{\mathrm{z}}^{D_{\mathrm{c}}}$(Doppler) of raindrops' velocity, and $V_{\mathrm{T}}(D_{\mathrm{c}}^{Z_{\mathrm{DR}}+D_{\mathrm{R}}})$ has the smallest difference to $v_{\mathrm{z}}^{D_{\mathrm{c}}}$(Doppler) compared with $V_{\mathrm{T}}(D_{\mathrm{c}}^{Z_{\mathrm{DR}}})$ and $V_{\mathrm{T}}(D_{\mathrm{c}}^{D_{\mathrm{R}}})$. Therefore, the characteristic size retrieval method based on polarimetric variables works well to represent the motion behavior of raindrops, and the fusion model based on $Z_{\mathrm{DR}} + D_{\mathrm{R}}$ has the best performance.

On the whole, the results of radar data test indicate that the retrieval of background wind velocity with the information of D_{c} is feasible, and further velocity verification should be made if we can deploy an accurate velocity measurement instrument in the high sky to get the background wind component $v_{\mathrm{z}}^{\mathrm{b}}$.

V. Conclusion

In this study, the raindrops' characteristic size D_{c} is defined, which corresponds to the strongest Doppler spectral component and can be used to retrieve the velocity of background wind in the further study. Then the relationship between D_{c} and polarimetric variables is analyzed for different radar bands and elevation angles to find a good retrieval model for D_{c}. Finally, experiments based on simulation results and field radar data show that:

1) both differential reflectivity (Z_{DR}) and the depolarization ratio (D_{R}) can serve as proxies for D_{c}, while D_{R} performs better than Z_{DR} in most cases, especially when the elevation angle is around 45°;

2) the fusion model based on Z_{DR} and D_{R} performs even better than D_{R} because it combines the advantages of Z_{DR} and D_{R};

3) the retrieval of background wind velocity with the information of D_{c} is feasible.

In this paper, the characteristic size of raindrops has been well defined and verified. This can build a good connection between the characteristic raindrops' velocity and the background wind velocity when the inertia of raindrops is considered. Because the integrating process is based on fitting and training the existing data, the performance of the fusion model is related to data quality and universality. Thus, efforts should be made to improve the applicability of the present method to other DSD models and observation data, and further to retrieve the background wind velocity based on the motion equation of the characteristic raindrops in more complex cases. This is on our near future work schedule.

References

[1] Y. Liu, S. Li, P. W. Chan, and D. Chen, "Empirical correction ratio and scale factor to project the extreme wind speed profile for offshore wind energy exploitation," *IEEE Transactions on Sustainable Energy*, vol. 9, no. 3, pp. 1030–1040, 2018.

[2] H. Gao, J. Li, P. W. Chan, K. K. Hon, and X. Wang, "Parameter-retrieval of dry-air wake vortices with a scanning doppler lidar," *Opt. Express*, vol. 26, pp. 16377–16392, Jun. 2018.

[3] R. Frehlich and N. Kelley, "Measurements of wind and turbulence profiles with scanning doppler lidar for wind energy applications," *IEEE Journal of Selected Topics in Applied Earth Observations and Remote Sensing*, vol. 1, no. 1, pp. 42–47, 2008.

[4] C. S. Ruf, G. Scott, and D. S. McKague, "Assessment of cygnss wind speed retrieval uncertainty," *IEEE Journal of Selected Topics in Applied Earth Observations and Remote Sensing*, vol. 12, no. 1, pp. 87–97, 2019.

[5] X. Chu, J. He, H. Song, Y. Qi, Y. Sun, W. Bai, W. Li, and Q. Wu, "Multimodal deep learning for heterogeneous gnss-r data fusion and ocean wind speed retrieval," *IEEE Journal of Selected Topics in Applied Earth Observations and Remote Sensing*, vol. 13, pp. 5971–5981, 2020.

[6] J. E. Stopa, A. A. Mouche, B. Chapron, and F. Collard, "Sea state impacts on wind speed retrievals from c-band radars," *IEEE Journal of Selected Topics in Applied Earth Observations and Remote Sensing*, vol. 10, no. 5, pp. 2147–2155, 2017.

[7] J. Kainulainen and *et al.*, "Airborne wind vector scatterometer for sea surface measurements," *IEEE Journal of Selected Topics in Applied Earth Observations and Remote Sensing*, vol. 12, no. 7, pp. 2470–2476, 2019.

[8] W. Huang, E. Gill, X. Wu, and L. Li, "Measurement of sea surface wind direction using bistatic high-frequency radar," *IEEE Transactions on Geoscience and Remote Sensing*, vol. 50, pp. 4117–4122, 10 2012.

[9] X. Liu, W. Huang, and E. W. Gill, "Wind direction estimation from rain-contaminated marine radar data using the ensemble empirical mode decomposition method," *IEEE Transactions on Geoscience and Remote Sensing*, vol. 55, no. 3, pp. 1833–1841, 2017.

[10] H. Chen and V. Chandrasekar, "Real-time wind velocity retrieval in the precipitation system using high-resolution operational multi-radar network," *Remote Sensing of Aerosols, Clouds, and Precipitation*, pp. 315–339, 2018.

[11] Y. Wang, M. Wei, Z. Wang, S. Zhang, and L. Liu, "Novel scanning strategy for future spaceborne doppler weather radar with application to tropical cyclones," *IEEE Journal of Selected Topics in Applied Earth Observations and Remote Sensing*, vol. 10, no. 6, pp. 2685–2693, 2017.

[12] L. Pfitzenmaier, Y. Dufournet, C. M. H. Unal, and H. W. J. Russchenberg, "Retrieving fall streaks within cloud systems using doppler radar," *Journal of Atmospheric and Oceanic Technology*, vol. 34, no. 4, pp. 905 – 920, 2017.

[13] S. Lovejoy and D. Schertzer, "Turbulence, raindrops and the l(1/2) number density law," *New Journal of Physics*, vol. 10, no. 7, p. 075017, 2008.

[14] T. A. Seliga and V. N. Bringi, "Potential use of radar differential reflectivity measurements at orthogonal polarizations for measuring precipitation," *Journal of Applied Meteorology and Climatology*, vol. 15, no. 1, pp. 69 – 76, 1976.

[15] C. W. Ulbrich, "Natural variations in the analytical form of the raindrop size distribution," *Journal of Applied Meteorology and Climatology*, vol. 22, no. 10, pp. 1764 – 1775, 1983.

[16] P. T. Willis, "Functional fits to some observed drop size distributions and parameterization of rain," *Journal of Atmospheric Sciences*, vol. 41, no. 9, pp. 1648 – 1661, 1984.

[17] G. Zhang, J. Vivekanandan, and E. Brandes, "A method for estimating rain rate and drop size distribution from polarimetric radar measurements," *IEEE Transactions on Geoscience and Remote Sensing*, vol. 39, no. 4, pp. 830–841, 2001.

[18] E. Gorgucci, V. Chandrasekar, V. N. Bringi, and G. Scarchilli, "Estimation of raindrop size distribution parameters from polarimetric radar measurements," *Journal of the Atmospheric Sciences*, vol. 59, no. 15, pp. 2373–2384, 2002.

[19] E. Gorgucci, V. Chandrasekar, G. Scarchilli, and S. Bolen, "Variation of mean raindrop shape derived from polarimetric radar measurements," *Atmospheric Research*, vol. 59-60, pp. 283–293, 2001. 13th International Conference on Clouds and Precipitation.

[20] H. R. Pruppacher and R. L. Pitter, "A semi-empirical determination of the shape of cloud and rain drops," *Journal of Atmospheric Sciences*, vol. 28, no. 1, pp. 86 – 94, 1971.

[21] M. Thurai, G. J. Huang, V. Bringi, W. Randeu, and M. Schoenhuber, "Drop shapes, model comparisons, and calculations of polarimetric radar parameters in rain," *Journal of Atmospheric and Oceanic Technology*, vol. 24, no. 6, pp. 1019 – 1032, 2007.

[22] D. Atlas, R. C. Srivastava, and R. S. Sekhon, "Doppler radar characteristics of precipitation at vertical incidence," *Reviews of Geophysics*, vol. 11, no. 1, pp. 1–35, 1973.

[23] A. Waldvogel, "The n0 jump of raindrop spectra.," *Journal of Atmospheric Sciences*, vol. 31, pp. 1067–1078, 04 1974.

[24] F. P. C. Caracciolo, F. Porcù, "Precipitation classification at mid-latitudes in terms of drop size distribution parameters," *Advances in Geosciences*, vol. 16, no. 6, pp. 11–17, 2008.

[25] L. S. Kumar, Y. H. Lee, and J. T. Ong, "Two-parameter gamma drop size distribution models for singapore," *IEEE Transactions on Geoscience and Remote Sensing*, vol. 49, no. 9, pp. 3371–3380, 2011.

[26] T. Islam, M. A. Rico-Ramirez, M. Thurai, and D. Han, "Characteristics of raindrop spectra as normalized gamma distribution from a joss–waldvogel disdrometer," *Atmospheric Research*, vol. 108, pp. 57–73, 2012.

[27] D. N. Moisseev and V. Chandrasekar, "Nonparametric estimation of raindrop size distributions from dual-polarization radar spectral observations," *Journal of Atmospheric and Oceanic Technology*, vol. 24, no. 6, pp. 1008 – 1018, 2007.

[28] Z. Liu, N. Jeannin, F. Vincent, and X. Wang, "Modeling the radar signature of raindrops in aircraft wake vortices," *Journal of Atmospheric and Oceanic Technology*, vol. 30, no. 3, pp. 470 – 484, 2013.

[29] J. Leinonen, "High-level interface to t-matrix scattering calculations: architecture, capabilities and limitations," *Opt. Express*, vol. 22, pp. 1655–1660, Jan 2014.

[30] A. T. Zadeh, M. Mälzer, J. Simon, S. Beck, J. Moll, and V. Krozer, "Range–doppler analysis for rain detection at ka-band: Numerical and experimental results from laboratory and field measurements," *IEEE Journal of Selected Topics in Applied Earth Observations and Remote Sensing*, vol. 13, pp. 1027–1033, 2020.

[31] G. J. Huang, V. N. Bringi, and M. Thurai, "Orientation angle distributions of drops after an 80-m fall using a 2d video disdrometer," *Journal of Atmospheric and Oceanic Technology*, vol. 25, no. 9, pp. 1717 – 1723, 2008.

[32] V. N. Bringi, M. Thurai, and D. A. Brunkow, "Measurements and inferences of raindrop canting angles," *Electronics Letters*, vol. 44, no. 24, pp. 1425–1426, 2008.

[33] V. Bringi and V. Chandrasekar, *Polarimetric Doppler Weather Radar: Principles and Operations*. Cambridge University Press, 10 2001.

[34] A. Ryzhkov, S. Y. Matrosov, V. Melnikov, D. Zrnic, P. Zhang, Q. Cao, M. Knight, C. Simmer, and S. Troemel, "Estimation of depolarization ratio using weather radars with simultaneous transmission/reception," *Journal of Applied Meteorology and Climatology*, vol. 56, no. 7, pp. 1797 – 1816, 2017.

[35] A. Ryzhkov, P. Zhang, Q. Cao, S. Matrosov, V. Melnikov, and M. Knight, "Measurements of circular depolarization ratio with the radar with simultaneous transmission / reception,"

[36] S. Y. Matrosov, C. G. Schmitt, M. Maahn, and G. de Boer, "Atmospheric ice particle shape estimates from polarimetric radar measurements and in situ observations," *Journal of Atmospheric and Oceanic Technology*, vol. 34, no. 12, pp. 2569 – 2587, 2017.

[37] Matrosov, "Ice hydrometeor shape estimations using polarimetric operational and research radar measurements," *Atmosphere*, vol. 11, no. 1, p. 97, 2020.

[38] S. Y. Matrosov, A. V. Ryzhkov, M. Maahn, and G. D. Boer, "Hydrometeor shape variability in snowfall as retrieved from polarimetric radar measurements," *Journal of Applied Meteorology and Climatology*, vol. 59, no. 9, pp. 1–36, 2020.

[39] J. Yin, H. Chen, Y. Li, and X. Wang, "Clutter mitigation based on spectral depolarization ratio for dual-polarization weather radars," *IEEE J. Sel. Topics Appl. Earth Observ. Remote Sens.*, vol. 14, pp. 6131 – 6145, 2021.

[40] C. Cortes and V. Vapnik, "Support vector networks," *Machine Learning*, vol. 20, pp. 273–297, 1995.

[41] A. D. Mehr, V. Nourani, V. Khosrowshahi, and M. A. Ghorbani, "A hybrid support vector regression–firefly model for monthly rainfall forecasting," *International Journal of Environmental Science and Technology*, vol. 16, pp. 1–12, 05 2018.

[42] E. Olyaie, H. Z. Abyaneh, and A. D. Mehr, "A comparative analysis among computational intelligence techniques for dissolved oxygen prediction in delaware river," *Geoscience Frontiers*, vol. 008, no. 003, pp. 517–527, 2017.

[43] W. Chen, Z.-J. Fu, and C.-S. Chen, *Recent Advances in Radial Basis Function Collocation Methods*. 12 2013.

[44] M. N. Jebur, B. Pradhan, and M. S. Tehrany, "Manifestation of lidar-derived parameters in the spatial prediction of landslides using novel ensemble evidential belief functions and support vector machine models in gis," *IEEE Journal of Selected Topics in Applied Earth Observations and Remote Sensing*, vol. 8, no. 2, pp. 674–690, 2015.

[45] S. Das, A. Maitra, and A. Shukla, "Rain attenuation modeling in the 10-100 ghz frequency using drop size distributions for different climatic zones in tropical india," *Progress In Electromagnetics Research B*, vol. 25, pp. 211–224, 01 2010.

[46] D. Sumbiri and T. J. O. Afullo, "Optimized rain drop size distribution model for microwave propagation for equatorial africa," *SAIEE Africa Research Journal*, vol. 111, no. 1, pp. 22–35, 2020.

[47] T. J. Schuur, A. V. Ryzhkov, D. S. Zrnić, and M. Schoenhuber, "Drop size distributions measured by a 2d video disdrometer: Comparison with dual-polarization radar data," *Journal of Applied Meteorology*, vol. 40, no. 6, pp. 1019 – 1034, 2001.

[48] C. A. Knight, L. J. Miller, and R. A. Rilling, "Aspects of precipitation development in trade wind cumulus revealed by differential reflectivity at s band.," *Journal of the Atmospheric Sciences*, vol. 65, no. 8, pp. 2563 – 2580, 2008.

[49] J. Yin, P. Hoogeboom, C. Unal, H. Russchenberg, F. van der Zwan, and E. Oudejans, "Uav-aided weather radar calibration," *IEEE Trans. Geosc. Remote Sens.*

[50] G. Teschke and V. Lehmann, "Mean wind vector estimation using the velocity–azimuth display (vad) method: an explicit algebraic solution," *Atmospheric Measurement Techniques*, vol. 10, no. 9, pp. 3265–3271, 2017.

Yunli Peng was born in 1997. She received the B.E. degree in Chengdu University of Information Technology, Chengdu, China, in 2019. She is currently working toward the M.E. degree in the College of Electronic Science and Engineering, National University of Defense Technology, Changsha, China, all in electronic and communication engineering.

Her research interests include the radar characteristics and the detection of distribution soft target.

Jianbing Li (S'08–M'10–SM'16) was born in 1979. He received the B.E. and M.E. degrees in Aerospace Science from the College of Aerospace Science and Engineering, National University of Defense Technology (NUDT), China, in 2002 and 2004, respectively, and the Ph.D. degree in information and communication engineering for his work on the analysis of wake vortices' scattering characteristics from the College of Electronic Science and Engineering, NUDT, in December 2010.

He is currently working as full professor in the College of Electronic Science and Engineering, NUDT. His research interests include the radar characteristics and detection of distributed soft target.

Dr. Li Ph.D. dissertation was awarded as a candidate of the National Outstanding Ph.D. dissertations in China in 2013. He received outstanding scientific and technical worker award of Chinese Institute of Electronics, and was also elected as an Outstanding Young Scholar in Hunan Province, China.

Jiapeng Yin received the B.Sc. degree in information engineering from the National University of Defense Technology (NUDT), Changsha, China, in 2012, and the Ph.D. degree in atmospheric remote sensing from the Delft University of Technology, Delft, The Netherlands, in 2019.

He is currently an Assistant Professor with the College of Electronic Science and Technology, NUDT. His research interests include radar polarimetry, polarimetric weather radar, radar signal processing, and radar calibration.

Pak Wai Chan is an Assistant Director of the Hong Kong Observatory responsible for weather forecasting and warning services for the public. Before that position, Mr. Chan has been working at the Hong Kong International Airport for over 20 years, with research and operational efforts in airport meteorological instrumentation, low level windshear and turbulence alerting, and high resolution numerical weather prediction.

He is a visiting professor of a number of universities in mainland China and an adjunct associate professor of the University of Hong Kong. He is a fellow of the Royal Meteorological Society and a Chartered Meteorologist. He has published more than 260 papers in SCI journals, with a significant portion of the papers focusing on the applications at the airport. He is a vice chair of the Expert Team of Upper Air Measurement at World Meteorological Organization and a chair of a working group of International Civil Aviation Organization in Asian region.

Wai Kong joined the Hong Kong Observatory since 2009. He is currently responsible for the provision of weather monitoring, forecasting and warning services for the public and government departments, and coordinating the development and implementation of forecasting services on high-impact extreme weather.

He has also been worked for the weather radar operation, calibration and maintenance of the Hong Kong Observatory for 10 years, overseeing the development of new radar applications and radar related researches, experiments and trainings. He is the member of the Joint Expert Team on Operational Weather Radar at the World Meteorological Organization.

Xuesong Wang was born in 1972. He received the B.Sc. and Ph.D. degrees from the College of Electronic Science and Engineering, National University of Defense Technology (NUDT), Changsha, China, in 1994 and 1999, respectively.

He is currently a Professor with NUDT, where he is also the Dean of the College of Science. His research interests concentrate on radar information processing and target recognition.

Dr. Wang is also a fellow of the Chinese Institute of Electronics. His Ph.D. dissertation was awarded as one of the 100 excellent Ph.D. dissertations in China, 2001 (two years after his graduation).